Mechanisms of the Cu(I)-catalyzed intermolecular photocycloaddition reaction revealed by optical and X-ray transient absorption spectroscopies

Gethmini K. Jayasekara,[1] Cali Antolini,[1] Melissa A. Smith,[1] Danielle J. Jacoby,[1] Jacqueline Escolastico,[2] Nathan Girard,[2] Benjamin T. Young,[2] and Dugan Hayes*[1]

[1]Department of Chemistry, University of Rhode Island, 45 Upper College Road, Kingston, RI 02881, USA

[2]Department of Physical Sciences, Rhode Island College, 600 Mt Pleasant Ave., Providence, RI 02908, USA

ABSTRACT: The [2 + 2] photocycloaddition provides a simple, single-step route to cyclobutane moieties that would otherwise be disfavored or impossible due to ring strain and/or steric interactions. We have used a combination of optical and X-ray transient absorption spectroscopies to elucidate the mechanism of the Cu(I)-catalyzed intermolecular photocycloaddition reaction using norbornene and cyclohexene as model substrates. We find that for norbornene, the reaction proceeds through an initial metal-to-ligand charge transfer (MLCT) state that persists for 18 ns before the metal returns to the monovalent oxidation state. The Cu K-edge spectrum continues to evolve until ~5 μs and then remains unchanged for the 50 μs duration of the measurement, reflecting product formation and ligand dissociation. We hypothesize that the MLCT transition and reverse electron transfer serve to sensitize the triplet excited state of one of the norbornene ligands, which then dimerizes with the other to give the product. For the case of cyclohexene, however, we do not observe a charge transfer state following photoexcitation and instead find evidence for an increase in the metal-ligand bond strength that persists for several ns before product formation occurs. This is consistent with a mechanism in which ligand photoisomerization is the initial step, which was first proposed by Salomon and Kochi in 1974 to explain the stereoselectivity of the reaction. Our investigation reveals how this photocatalytic reaction may be directed along strikingly disparate trajectories by only very minor changes to the structure of the substrate.

INTRODUCTION

Aside from radical initiation and photoinduced charge transfer (i.e., photoredox), the use of photochemistry in organic synthesis remains restricted to a small number of well-known reactions with relatively narrow scope. Among the group of established photochemical reactions in organic synthesis, "[t]he [2 + 2] photocycloaddition is undisputedly the most important and most frequently used," according to a recent review by Bach and coworkers.[1] This reaction is particularly useful in many natural product syntheses, where it provides a single-step route to challenging fused multicyclic and/or heterocyclic moieties,[2−4] and it was famously used as a key step in the landmark syntheses of caryophyllene[5] and cubane.[6] More recently, Jiang *et al.*[7] and Skubi *et al.*[8] reported new catalytic platforms for the [2 + 2] photocycloaddition with unparalleled regio- and/or stereoselectivity, demonstrating that even after more than a century, the potential scope of this reaction has still not been fully explored.

Because the π-π* transitions of unconjugated olefins appear in the vacuum ultraviolet (UV) and exhibit poor intersystem crossing (ISC) yields, photocycloadditions of such substrates are typically accomplished using a triplet sensitizer or a Cu(I) salt as a catalyst. Cu(I) bis(olefin) complexes exhibit absorption bands in the near-UV that may be excited to drive the reaction with quantum yields greater than 60%,[9] and a similar approach has been recently used to accommodate carbonyl substrates in a Cu(I)-catalyzed analog of the Paternò-Büchi reaction.[10] Nevertheless, while this cheap, earth-abundant catalyst broadens the scope of this reaction, it also brings its own set of limitations. For example, intermolecular cycloadditions are only possible when at least one of the substrates possesses ring strain at the position of the target alkene,[11] while intramolecular cycloadditions are essentially only possible for 1,6-dienes.[12] Although computational chemistry could help identify potential substrates and/or catalysts capable of overcoming these shortcomings, such work first requires a robust understanding of the reaction mechanism.

The Cu(I)-catalyzed intermolecular olefin photocycloaddition was first reported in 1965 by McKeon and coworkers, who used quantum yield measurements to conclude that the photocatalytic dimerization of norbornene in the presence of CuBr proceeds through photoexcitation of the 1:1 metal:ligand species, which then reacts with two additional norbornene molecules in solution to give the dimer

and the ground state 1:1 complex.[13,14] In 1973, Salomon and Kochi showed that the superior solubility of Cu(I) trifluoromethanesulfonate (CuOTf) and its olefin complexes in ethereal solvents results in an order of magnitude improvement in quantum yield over Cu(I) halides.[15] The improved solubility also permitted a broader range of concentration-dependent quantum yield measurements, from which the authors concluded that the reaction actually proceeds exclusively from the pre-associated Cu(I) bis(norbornene) complex.[9] Kochi and coworkers also explained the *trans-anti-trans* stereoselectivity of the CuOTf-catalyzed photodimerizations of cyclohexene and cycloheptene by proposing a mechanism invoking an initial ligand photoisomerization followed by cycloaddition with a ground state substrate molecule,[11] consistent with the photoisomerization of the Cu(I) complex of *cis-cis*-1,5-cyclooctadiene to the *cis-trans* form observed earlier by Whitesides.[16]

Despite this previous work, the mechanisms of these reactions remain unclear, with even the nature of the photochemically active optical transition(s) disputed. Salomon outlined several potential concerted and sequential mechanisms for the dimerization of norbornene invoking metal-to-ligand charge transfer (MLCT) or ligand-to-metal charge transfer (LMCT) states,[17] with the formation of the organocopper carbenium intermediate via the latter pathway termed "photocupration".[18] In 1985, Geiger and Ferraudi performed flash photolysis studies of the Cu(I)-catalyzed photopolymerization of ethylene and photoisomerization of cyclooctadiene and observed transient species with lifetimes ranging from nanoseconds to milliseconds that they assigned primarily to biradical alkyl copper intermediates by comparison to stable organocopper species.[19] This work strongly suggested that the metal plays a crucial role beyond simply templating the otherwise bimolecular reaction and/or promoting ISC following a ligand centered ($\pi \rightarrow \pi^*$) transition. Electronic structure calculations by Baerends and coworkers two years later provided compelling evidence for a mechanism in which such a Cu(I) biradical forms from an initially populated MLCT excited state,[20] but to date there is still no direct experimental evidence for any single reaction mechanism.

While optical transient absorption (OTA) spectroscopy has been used to investigate metal-free photocycloadditions of enones[21,22] and quinolones,[23] similar efforts have not been reported for the Cu(I)-catalyzed photochemical dimerization of olefins. In this work, we leverage the strengths of both OTA and X-ray transient absorption (XTA) to observe the excited state dynamics of such reactions in real time and thereby obtain clear pictures of their respective mechanisms. XTA allows us to track the oxidation state and ligation environment of the copper center, while OTA provides a probe of transient Cu(II) species with sub-ps resolution. We find that norbornene and cyclohexene, model substrates differing by only a single methylene bridge, exhibit strikingly disparate spectral features and dynamics. The distinct photodimerization mechanisms suggested by these results have important implications for understanding and expanding the scope of this class of reactions.

RESULTS AND DISCUSSION

Steady-state photochemical characterization. The photocycloaddition rates of norbornene and cyclohexene in THF in the presence of catalytic CuOTf (1 mol%) were qualitatively compared by monitoring loss of the starting materials and appearance of the dimers upon UV irradiation (254 nm) with ^{1}H NMR (see Supporting Information (SI) for details). The olefin peaks at 6.0 ppm (norbornene) and 5.6 ppm (cyclohexene) provide clear spectroscopic handles for measuring conversion (Figs. S1-S2). Although this method cannot directly provide quantum yields, the bulk dimerization rates obtained by peak integration differ only by a factor of ~2 (Fig. 1A), and both reactions approach complete conversion in 168 hours (we note that the apparent rate constants are not proper first order rate constants but instead depend on the ligand association constants, the molar extinction coefficients, and the quantum yields of the reactions[24]). After 7 days, the reaction mixtures were extracted into pentane and analyzed by ^{1}H NMR to confirm formation of the dimers.

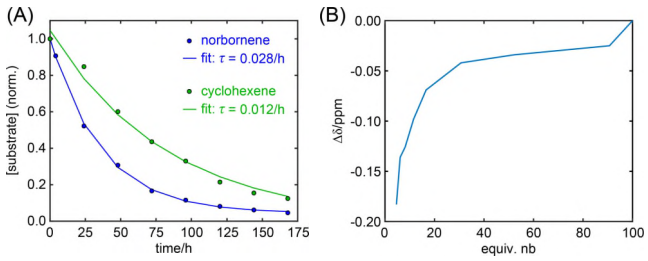

Figure 1. (A) Disappearance of norbornene and cyclohexene vs. time under constant incoherent irradiation at 254 nm in the presence of 1 mol% CuOTf in THF. Data points are shown with first order rate law fits overlain. (B) Change in ^{1}H NMR chemical shift of norbornene olefin peak as a function of excess norbornene concentration relative to CuOTf as measured throughout the photochemical reaction shown in panel A.

The chemical shift of the olefin peak in norbornene is known to be sensitive to the presence of Cu(I), moving steadily upfield as the concentration of Cu(I) increases relative to that of norbornene.[25] Because ligand exchange occurs on the timescale of the NMR measurement, this behavior is observed even when norbornene is present at very high excess concentrations; indeed, this gradual shift is apparent in the spectra acquired throughout the 7 day irradiation (Fig. S1), during which the ligand was present in >10-fold excess. Before irradiation, however, the peak appears at 5.988 ppm, which is essentially identical to the 5.989 ppm shift observed for norbornene alone. The chemical shift relative to that of norbornene alone is plotted vs. equivalents of substrate in Fig. 1B, showing strong upfield deviations at <30 equivalents but converging to zero at higher concentrations. Though we have not sought to extract equilibrium constants for coordination of one and two norbornene ligands from this data, the asymptotic nature of the curve indicates that the Cu(I) exists largely as the pre-reactive bis(olefin) complex at the high concentrations of ligand used in all experiments reported here. Notably, Salomon and Kochi found the quantum yield for the

photodimerization of a 0.4 M solution of norbornene as a function of CuOTf concentration to plateau at ~12 mM,[9] further supporting this conclusion.

X-ray transient absorption. XTA measurements at the Cu K-edge were performed at beamline 11-ID-D at the Advanced Photon Source (APS, Argonne National Laboratory). The synchronization of the laser and X-ray pulses and the detection scheme have been described previously,[26] and further details are provided in the SI. Briefly, a 6 mM solution of CuOTf in THF with no substrate or 0.6 M norbornene was circulated using a peristaltic pump to deliver a liquid jet at the sample position, where the laser and X-ray beams were spatially overlapped at a shallow angle. The solutions were constantly purged with N_2, and the sample chamber was carefully sealed to prevent oxidation of Cu(I) by air. The third harmonic of the 3 kHz output of a Ti:sapphire laser provided 100 fs pulses at 267 nm, which were used to trigger the photocycloaddition reaction. X-ray absorption near edge structure (XANES) spectra were then obtained by scanning the energy of the ~1 eV monochromatized X-ray beam and measuring the total X-ray fluorescence from the sample for each X-ray pulse (6.5 MHz) using avalanche photodiodes. Because XANES is an element-specific technique, samples could be prepared in 50-fold excess of substrate to drive the equilibrium[9] between Cu^+, $[Cu(olefin)]^+$, and $[Cu(olefin)_2]^+$ predominantly toward $[Cu(olefin)_2]^+$ and keep the concentration of substrate approximately constant over the 12 h measurement windows.

Ground state (i.e., "laser off") XANES spectra of THF solutions of CuOTf alone and CuOTf with norbornene (nb) are shown in Fig. 2 with difference spectra ("laser on" minus "laser off") acquired at three pump-probe delay times plotted underneath. The K-edge spectrum of a Cu(I) complex is characterized by one or more distinct peaks along the rising edge that correspond to the dipole-allowed 1s→4p transitions. The number, amplitude, and separation of these peaks is keenly sensitive to the coordination geometry about the metal center and the degree of mixing between the Cu 3d/4p orbitals and unoccupied ligand orbitals.[27,28] The features in the region about the most intense peak in the spectrum (known as the white line) are typically attributed to multiple scattering events,[29,30] although there may also be some contribution from transitions to higher lying bound states.[31] An additional pre-edge band is present in d^9 Cu(II) species, which corresponds to nominally dipole-forbidden 1s→3d transitions that gain intensity through 3d/4p mixing.[32] The edge energy observed for Cu(II) species is also typically 2-3 eV higher than for similar Cu(I) species due to the greater effective nuclear charge experienced by the 1s electrons.[33]

The CuOTf difference spectrum at 100 ps shows a broad excited state absorption (ESA) feature in the 1s→4p region along the edge as well as a sharp ground state bleach (GSB) at 8.981 keV and oscillatory features across the multiple scattering region. By the arrival of the subsequent probe pulse 153 ns later, the sharp GSB has mostly disappeared, while the other features have decayed only moderately. The bottom spectrum, which is averaged over 27 probe pulses spanning 2-6 μs to provide improved signal-to-noise, is essentially unchanged from the 153 ns spectrum. The CuOTf + nb difference spectrum at 100 ps, however, shows two prominent GSB peaks along the edge but no discernable features beyond the white line. By 153 ns the difference appears essentially flat, while the 2-6 μs averaged spectrum shows a weak but broad ESA feature in the 1s→4p region and a slight bleaching of the white line.

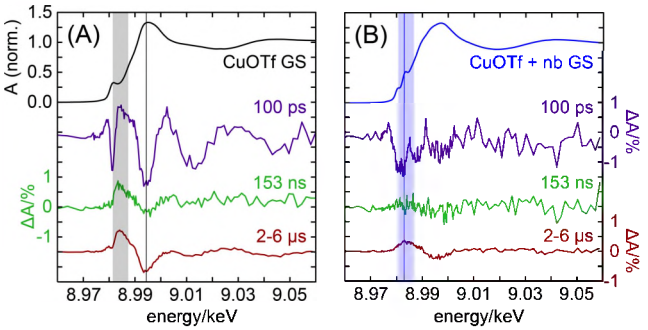

Figure 2. Ground state (GS) and difference Cu K-edge XANES spectra of 6 mM CuOTf in THF (A) and 6 mM CuOTf and 0.6 M norbornene in THF (B) at several pump-probe delay times. The probe energies for which the short- and long-time kinetics are plotted in Fig. 4 are indicated by vertical lines and bars, respectively.

Approximate XANES spectra of the transient species (Fig. 3) were obtained by subtracting a fractional amount of the "laser-off" spectra from the corresponding "laser-on" spectra and renormalizing the resulting data (see SI for details). An excited state fraction of 4% was used for all spectra, estimated from the laser pulse energy and spot size and sample optical density. Because both samples show no further spectral evolution after ~10 μs, a transient spectrum with excellent signal-to-noise could be obtained by averaging all 65 X-ray probe pulses arriving between 25 and 35 μs after the laser pump pulse. These spectra (peach) are plotted with the ground state spectrum (black or blue) in each panel of Fig. 3 as reference points for analyzing the 100 ps (cyan) and 153 ns (green) spectra, which were obtained from only a single probe pulse per pump pulse.

The 100 ps CuOTf spectrum shows clear changes in the 1s→4p region but no apparent shift in the edge energy, as would be expected to accompany a charge transfer. There is also no evidence of a 1s→3d pre-edge feature at ~8.977 keV. Instead, a new peak appears at ~8.980 keV that is consistent with a Cu 1s→O *n* MLCT transition that gains intensity due to strong mixing between the O *n* and Cu $4p_z$ orbitals,[34–36] though detailed computational work would be necessary to support such an assignment. By 153 ns, the spectrum appears essentially identical to that observed at all later times, with a prominent 1s→4p ESA and a bleaching of the white line but still no evidence of an edge shift. This spectrum and the corresponding difference spectra in Fig. 2 are in excellent qualitative agreement with those presented by Solomon and coworkers for Cu(I) species with progressively lower coordination numbers.[27] Thus, we conclude that the optical transition does not involve the Cu(I) center directly but is instead an *n*→3s transition at one of

the weakly associated THF ligands, resulting in photodissociation. The lower-coordinate Cu(I) center then reaches a metastable state within 153 ns, and equilibration back to the fully coordinated ground state species does not occur within the 45 μs experimental window.

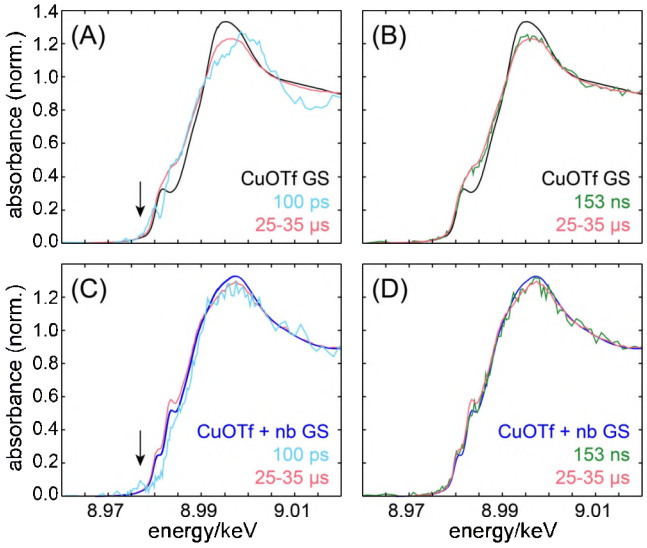

Figure 3. Transient Cu K-edge XANES spectra calculated from laser-on and laser-off spectra of 6 mM CuOTf in THF (A and B) and 6 mM CuOTf and 0.6 M norbornene in THF (C and D) obtained at several pump-probe delay times (cyan, green, and peach). Ground state spectra (black and blue) are also plotted for reference. The energy of the pre-edge feature that appears at 100 ps only in the sample with norbornene (8.977 keV) is indicated by a vertical arrow.

The 100 ps CuOTf + nb spectrum, however, shows the hallmarks of a $3d^9$ Cu(II) center: a pre-edge feature at 8.977 keV corresponding to the presence of a 3d hole, and a hypsochromic edge shift corresponding to the increase in oxidation state and stabilization of the 1s electrons. The shoulder at 8.9840 keV is also consistent with the characteristic 1s→4p + LMCT shakedown transition of Cu(II) species.[31,37,38] Accordingly, we can unambiguously conclude that the excited state of the $[Cu(nb)_2]^+$ complex 100 ps after excitation at 267 nm is an MLCT state. Within 153 ns, the transient spectrum is indistinguishable from the ground state spectrum, indicating that reverse electron transfer has returned the metal to a monovalent state. However, the spectrum continues to evolve over the next several μs, ultimately giving a metastable spectrum exhibiting the same 1s→4p ESA and bleaching of the white line observed for the CuOTf sample. Because these features are consistent with decreased coordination number, the final spectrum may be assigned to the Cu(I) species present following product formation and dissociation. The Cu(I) species observed at 153 ns thus corresponds to a reaction intermediate that forms following reverse electron transfer from the initially prepared MLCT state.

Time scans with ~50 ps resolution were also performed at the probe energy for which ΔA at 100 ps was of greatest magnitude for each sample (indicated by vertical lines in Fig. 2: 8.9944 keV for CuOTf, 8.9825 keV for CuOTf + nb), as shown in Fig. 4A. Because these kinetic traces were acquired at different spectral regions for the two samples, caution must be used when making any direct comparison; nevertheless, each trace still provides important information on the excited state dynamics of the corresponding system. In particular, the bleach in the CuOTf sample recovers monoexponentially with a time constant of 320 ps (fit shown in red), while the bleach in the CuOTf + nb sample appears essentially static out to 2 ns. But while ps/ns dynamics could only be monitored at one probe energy at a time, the 6.5 MHz X-ray pulse train provides full XTA spectra out to 45 μs in steps of 153 ns. To improve signal-to-noise, the difference was integrated over the entire ESA peak observed at >2 μs in both datasets (integration regions indicated by vertical bars in Fig. 2), and the kinetic traces are plotted in Fig. 4B. Both show a few-μs rise time (3.8 μs for CuOTf, 2.7 μs for CuOTf + nb), but CuOTf also shows a substantial impulsive ESA component. CuOTf + nb shows no evidence of an impulsive ESA, instead showing only an impulsive GSB that decays back to the baseline by the arrival of the next X-ray pulse due to the forward and reverse photoinduced electron transfer events. Thus, while some slow equilibration process likely occurs in the CuOTf sample on the μs time scale following excitation, ligand photodissociation occurs within only 320 ps. For CuOTf + nb, on the other hand, product formation and dissociation occur with a long time constant of 2.7 μs.

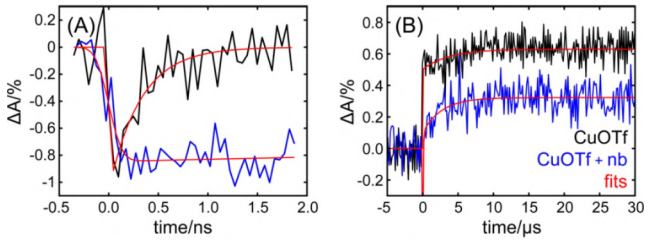

Figure 4. Fast (A) and slow (B) Cu K-edge kinetic traces measured for 6 mM CuOTf in THF (black) and 6 mM CuOTf and 0.6 M norbornene in THF (blue) and corresponding fits (red). The probe energies at which the traces were measured in panels A and B are indicated in Fig. 2 by vertical lines and bars, respectively.

XTA difference spectra of CuOTf with cyclohexene (ch) at various delay times are presented in Figs. 5A-C. The ground state spectrum of CuOTf + ch is shown alongside those of CuOTf and CuOTf + nb in Fig. S5; we tentatively ascribe the differences observed in the 1s→4p region between the two olefin complexes to the respective D_{2d} vs. D_{2h} geometries of the optimized bis(nb) and bis(ch) complexes, though further computational work is required to confirm this origin. The spectrum at 100 ps shows neither the pre-edge ESA at 8.977 keV nor the hypsochromic edge shift observed for CuOTf + nb, indicating that the optical transition is not an MLCT. There is no evidence either of a bathochromic edge shift, indicating that the transition is also not an LMCT. The only clear feature is a bleaching of the 1s→4p peak at 8.9806 keV. By 153 ns, the difference spectrum appears essentially flat, while at later delay times it resembles the μs difference spectra of the CuOTf and

CuOTf + nb systems (Fig. 2). The GSB at 8.9806 keV partially recovers with a time constant of 280 ps but then persists beyond 2 ns (Fig. 5D), while the ESA observed at late delay times grows with a time constant of 5.5 μs (Fig. 5E). These observations are consistent with a change in the metal-ligand binding on the ps and ns time scales and product formation and ligand dissociation at a rate comparable to that observed for CuOTf + nb.

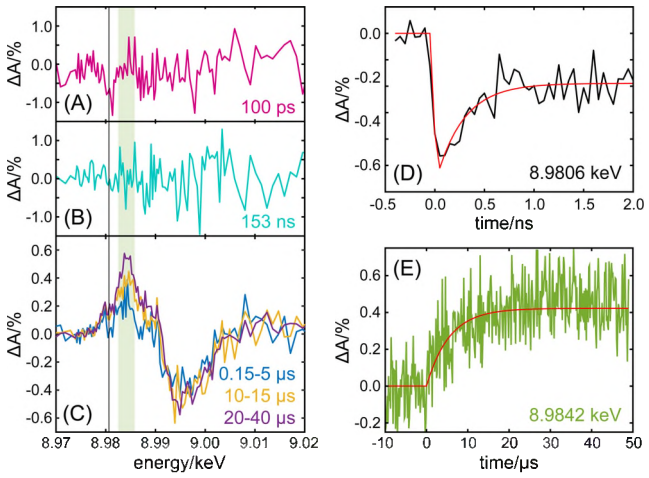

Figure 5. (A) – (C) X-ray transient absorption difference spectra of 3 mM CuOTf and 0.3 M cyclohexene in THF at various pump-probe delay times. (D) Short-time kinetic trace measured at the probe energy indicated by the vertical line in panels A-C. (E) Long-time kinetic trace averaged over the probe bandwidth indicated by the vertical bar in panels A-C.

Optical transient absorption. Although it is clear from the spectrum in Fig. 3 that $[Cu(nb)_2]^+$ is in a Cu(II)* MLCT state at 100 ps, it is possible that a different state is populated immediately following photoexcitation. The temporal resolution achievable for XTA experiments at storage ring light sources such as the APS is typically limited to ~100 ps, and thus we investigated the ultrafast dynamics of the reaction using fs OTA. Although this method does not have the element specificity of XTA, the Cu(II)* state may be easily identified by the appearance of a band in the visible regime, across which the ground state $[Cu(nb)_2]^+$ complex exhibits essentially no absorption. This band could correspond to the Cu(II) ligand field transition, absorption by the norbornene radical anion, or some combination of the two; further work is required for a conclusive assignment to be made.

OTA spectra at representative delay times are shown in Fig. 6A. A persistent ESA is observed at negative delay times (blue), and it is also observed in neat THF (gray) at both positive and negative delay times (Fig. S7). The increasing intensity of this ESA band at longer probe wavelengths is consistent with previously reported spectra of ionized THF generated by pulse radiolysis,[39,40] and thus we assign it to the long-lived species produced by multiphoton ionization of the solvent[41] (i.e., solvent radical cations and solvated electrons). A much stronger ESA band consistent with the Cu(II)* state, however, appears between 450 and 650 nm at positive times, growing in amplitude and shifting toward shorter wavelengths over the first several ps until reaching a maximum amplitude at ~10 ps. This non-impulsive behavior is highlighted by the kinetic trace shown in the inset (data averaged over the 468-482 nm probe region indicated by the gray bar). After this time the spectrum remains essentially unchanged, decaying only slightly over the 2 ns delay window.

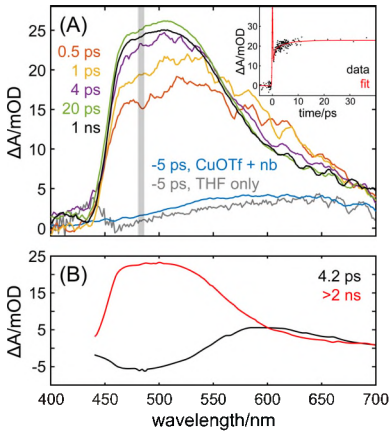

Figure 6. (A) Optical transient absorption spectra of 6 mM CuOTf and 0.6 M norbornene in THF at representative pump-probe delay times, showing the growth of the ESA signal over the first several ps. The -5 ps spectra of both the Cu + nb sample in THF (blue) and neat THF (gray) show a weak ESA signal due to the multiphoton ionization of the solvent. The early-time kinetic trace taken from the probe region indicated by the vertical bar is shown in the inset with the corresponding multi-exponential fit. (B) Decay-associated spectra of CuOTf + nb obtained from a global fit of the optical transient absorption data.

Decay-associated spectra are plotted in Fig. 6B (see SI for details). The sub-ps signal is dominated by a strong coherent artifact (Fig. S7) and likely includes contributions from several other processes, including thermalization of the excited state species, solvent reorganization, and geminate recombination of solvated electrons and solvent radical cations; accordingly, we do not attempt to analyze the OTA spectra within this window. However, the data beyond 1 ps may be fit across the entire probe spectrum with only two components: a fast component with an average time constant of 4.2 ps (black) and a slow component with a time constant much longer than the 2 ns delay window (red). While the ESA on the red side of the 4.2 ps component likely contains contributions from ionized solvent dynamics, the OTA signal at wavelengths shorter than 500 nm may be ascribed entirely to the $[Cu(nb)_2]^+$ complex.

The negative signal in the 4.2 ps component in this region cannot be assigned to the partial recovery of the GSB, as the steady-state optical spectrum of this solution does not exhibit any absorption bands at visible wavelengths; although some absorption is observed at wavelengths >450 nm, this simply corresponds to the tail of the main UV absorption band, which decays smoothly out to ~650 nm (Fig. S4). However, because the sign of the OTA signal is positive at all probe wavelengths, the non-impulsive growth of the signal between 450 and 525 nm could correspond to 1)

stimulated emission from the thermalized singlet excited state and/or 2) spectral narrowing due to intramolecular vibrational redistribution. Crucially, no spectral evolution is observed after ~10 ps, meaning the 4.2 ps relaxation must yield the thermalized ^{3}MLCT state observed by XTA at 100 ps. ISC rates of a few ps have been reported for the MLCT states of many Cu(I) complexes,[33,42–44] but in the absence of ultrafast emission spectra, we cannot conclusively assign the 4.2 ps component to either ISC from the thermalized ^{1}MLCT state or thermalization of the ^{3}MLCT state.

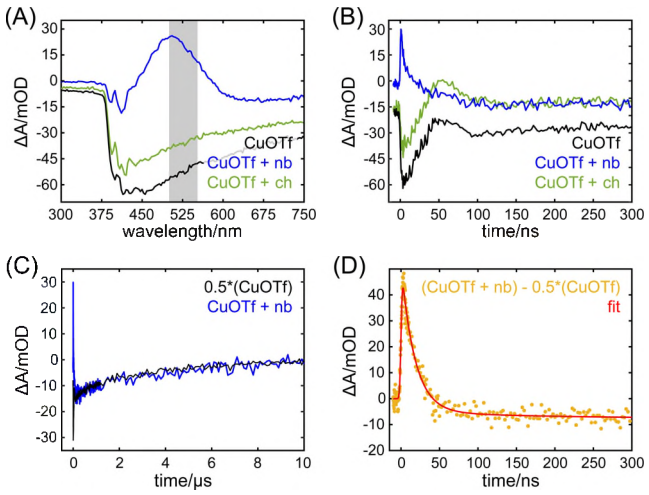

Figure 7. (A) Optical transient absorption spectra of 6 mM CuOTf in THF (black), 6 mM CuOTf and 0.6 M norbornene in THF (blue), and 6 mM CuOTf and 0.6 M cyclohexene in THF (green) averaged over a pump-probe delay window of 2.8 to 3.8 ns. (B) Kinetic traces obtained by averaging over the probe window indicated by the vertical bar in panel (A). (C) Long-time kinetic traces of CuOTf alone scaled by a factor of 0.5 and CuOTf + nb, highlighting the identical kinetics observed on the μs time scale for the different samples. (D) Kinetic trace of CuOTf + nb with the contributions from multiphoton solvent ionization subtracted (mustard) and the corresponding fit (red) to a single exponential decay and a persistent offset.

Because the XTA and fs-resolved OTA measurements could only provide lower and upper bounds for the lifetime of the ^{3}MLCT state (2 and 153 ns, respectively), we also performed ns-resolved OTA to determine the precise value. OTA spectra averaged over a delay window of 2.8-3.8 ns are shown in Fig. 7A for CuOTf only (black) and CuOTf with norbornene (blue) and cyclohexene (green), and corresponding kinetic traces obtained by averaging over the probe spectral region indicated by the vertical bar are shown in Fig. 7B. The CuOTf sample provides a convenient means of eliminating contributions to the CuOTf + nb signal from multiphoton ionization of the solvent. Scaling the CuOTf signal by 50% gives a kinetic trace that matches that of CuOTf + nb nearly perfectly after 100 ns across the remainder of the 10 μs delay window (Fig. 7C). Accordingly, we may subtract the scaled CuOTf trace from the CuOTf + nb trace to isolate contributions from the photocatalytic species. While the subtraction likely introduces some artifacts in the data, we only seek to obtain the time constant unique to the CuOTf + nb sample that is also apparent in the raw data (Fig. 7B). The subtracted data (Fig. 7D, mustard dots) is fit well (red trace) by a single exponential decay and a persistent negative component, giving a reverse electron transfer rate of 18 ns.

Meanwhile, it is clear from Figs. 7A-B that the ns-resolved OTA data obtained for CuOTf alone and CuOTf + ch are essentially identical to within a scaling factor. The signal is ~30% weaker for CuOTf + ch, demonstrating that while multiphoton solvent ionization still occurs in this sample, many photons are now being absorbed instead by the copper species. The lack of the strong ESA signal centered at 500 nm observed for the CuOTf + nb sample provides further evidence that a Cu(II)* transient species is not formed and thus the optical transition is not an MLCT. The OTA data alone for CuOTf + ch, however, are inconclusive.

Reaction mechanisms. Based upon the results presented above, we propose two distinct mechanisms for the [2 + 2] intermolecular photocycloaddition reactions of norbornene and cyclohexene, as illustrated by the Jablonski diagrams shown in Fig. 8. In the case of norbornene, the relevant ground state species is the singlet $[Cu(nb)_2]^+$ complex, labeled $^1S_0$. Photoexcitation at 267 nm brings this species to the Franck-Condon state on the ^{1}MLCT potential energy surface, characterized by an oxidized Cu(II) center coordinated by a norbornene and a norbornene radical anion ligand. This species undergoes ISC to the thermalized ^{3}MLCT state within 4.2 ps. Reverse electron transfer within 18 ns returns the copper center to the monovalent oxidation state, resulting in a reactive ligand-centered triplet biradical species (^{3}LC); understanding the nature of the metal-ligand binding in this species is the subject of ongoing work. Finally, the cycloaddition reaction proceeds within 2.7 μs to give the norbornene dimer and a coordinatively unsaturated Cu(I) species. We note, however, that while we favor the mechanism in which photocycloaddition proceeds from the ^{3}LC state as in the case of direct olefin excitation or triplet sensitization, we cannot rule out the possibility that the first C-C bond formation occurs in the ^{3}MLCT state prior to reverse electron transfer to give a metallacyclic intermediate.

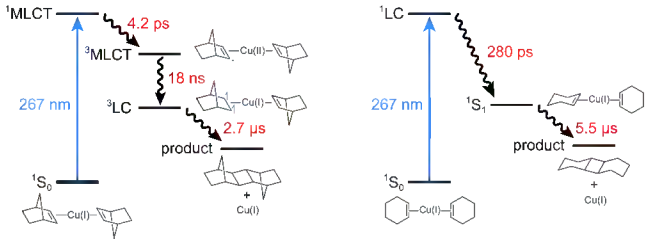

Figure 8. Jablonski diagrams for the Cu(I)-catalyzed [2 + 2] photocycloaddition reactions of norbornene (left) and cyclohexene (right).

While each of the intermediates and time constants given for norbornene are strongly supported by the XTA and OTA data, the cyclohexene system is notable for a *lack* of any clear OTA signal between 450 and 700 nm. Importantly, our NMR study of the photochemical dimerizations of norbornene and cyclohexene shows that the two

compounds convert to product on comparable time scales. We may thus rule out the possibility that the cyclohexene system simply does not exhibit an OTA signal due to prohibitively unfavorable branching between an unreactive majority species and a reactive minority species in the excited state. In conjunction with the XTA data, this allows us to confidently say that the photochemically relevant excited state species is not a charge transfer state, and the reaction thus proceeds through an entirely different mechanism than in the case of norbornene.

The cyclohexene photocycloaddition mechanism proposed by Kochi and coworkers invokes the *cis-trans* photoisomerization of a cyclohexene ligand as the initial step,[11] and this was later supported by further steady-state photochemical stereoselectivity experiments reported by Kropp *et al.*[45] Copper(I)[46,47] and other transition metals[48,49] are known to stabilize strained *trans*-cycloalkenes to furnish isolable species, and thus a transient *trans*-cyclohexene intermediate[50] is not unreasonable. Additionally, *trans*-cyclooctene exhibits stronger binding to Cu(I) than its *cis* counterpart,[51] presumably due to relief of strain.[52] While such an initial photoisomerization step is not directly supported by our OTA and XTA data, it is consistent with all of our observations. Thus, we propose the mechanism illustrated in Fig. 8, in which excitation at 267 nm yields a ^{1}LC ($\pi\rightarrow\pi^*$) Franck-Condon state. We tentatively assign the 280 ps time constant observed by XTA to the photoisomerization and re-binding of a cyclohexene ligand to give the $^1S_1$ intermediate, as the persistent bleaching of the 1s→4p peak beyond this time is consistent with stronger coordination, and other solution-phase photoisomerization reactions are known to occur on similar time scales.[53] However, it is also possible that the partial recovery of the bleach arises from differences in the coordination of the triplet and singlet ($\pi\rightarrow\pi^*$) states and thus corresponds to ISC, with isomerization and concomitant relaxation of the ($\pi\rightarrow\pi^*$) state occurring within the 2-153 ns window for which we do not have XTA data. Finally, as with norbornene, the cycloaddition reaction proceeds within a few μs to give the product and a coordinatively unsaturated Cu(I) species.

These two model systems help us understand why such a broad variety of reaction mechanisms have been proposed for Cu(I)-catalyzed [2 + 2] photocycloadditons: even very slight changes to the substrate (isomerizability in this case, but potentially also ring size/strain, sterics, inductive effects, etc.) can drive the reaction along diverging trajectories. Thus, while we have conclusively ruled out the possibility of a photocupration scheme involving a Cu(0) LMCT state for the dimerizations of norbornene and cyclohexene, such a mechanism could be operative for other olefins. Nevertheless, we believe that the MLCT and LC mechanisms outlined above are likely quite general for bridged bicyclic and monocyclic reactants, respectively.

Several questions regarding these reactions remain unanswered, however. In addition to the question of isomerization vs. ISC discussed above for cyclohexene, the provenance of the second monomer is uncertain for both substrates. Neither the XTA nor the OTA data provide evidence for a strictly pseudo-unimolecular reaction (as depicted in Fig. 8 for the sake of simplicity) or a mechanism in which the excited state complex and/or dissociated reactive ligand species (the triplet biradical for norbornene and the *trans* isomer for cyclohexene) reacts in a truly bimolecular fashion with a ground state monomer to give the product and Cu(I) coordinated to a single monomer. While Salomon and Kochi favored the pseudo-unimolecular mechanism for norbornene, they could not conclusively discount the possible bimolecular schemes either.[9] A thorough analysis using, for example, the ^{1}H NMR data shown in Fig. 1A is beyond the scope of this work, as the kinetic model must include: 1) equilibrium constants for the formation of the mono(olefin) and bis(olefin) species, 2) extinction coefficients of Cu(I) with zero, one, and two olefin ligands, and 3) the quantum yield of the reaction in the limit of infinite olefin concentration. Nevertheless, we may qualitatively consider the expected behavior for both cases. Under the low light intensity used in the steady-state photochemistry experiments, the concentration of reactant for a unimolecular mechanism should fall at a constant rate.[54] However, if we assume the equilibrium constants are >>1 and >1 M^{-1} for the formation of the mono(olefin) and bi(olefin), respectively (*vide supra*),[9] the rate of the reaction should also show first order dependence with respect to concentration of olefin at moderate concentrations (~0.01-1 M). Thus, we expect the apparent kinetics for this mechanism to follow a first order rate law at the concentrations investigated here. In the case of a truly bimolecular reaction, the reaction rate would depend on the concentration of both the bis(olefin) and the free olefin, and the apparent kinetics would follow a second order rate law. The data obtained from integration of the NMR spectra clearly do not follow second order kinetics but are well modeled using first order kinetics (Fig. S3). This strongly suggests that Cu(I) indeed also serves as a template in these reactions, though further work is required to prove this conclusively.

Perhaps the most important outstanding questions are those related to the metal-ligand bonding in the various intermediate species, and additional XTA experiments offer the possibility of addressing these directly. In particular, the loss of ($3d\rightarrow\pi^*$) back bonding that would accompany the change in hapticity in going to an alkyl copper species should be evident in the intensity of the pre-edge,[28,35] though many hours to even days of signal averaging would likely be required to resolve changes in such a weak feature with single X-ray bunch averaging (i.e., at early delay times). Extended X-ray absorption fine structure (EXAFS) analysis may also be possible with longer signal averaging, which could distinguish between linear and metallacyclic species and provide coordination numbers.

CONCLUSIONS

We have shown that the Cu(I)-catalyzed [2 + 2] photocycloaddition of norbornene proceeds following the population of a Cu(II)* MLCT state that persists for 18 ns before relaxing to the LC state that ultimately combines with a ground state monomer to provide the dimer. The LC state is most likely a triplet biradical species, which suggests that

the Cu(I) catalyst essentially serves as a pseudo-intramolecular triplet sensitizer. Because the ^{1}MLCT state may be accessed at near-UV wavelengths, it provides a path by which the high-energy (and presumably short-lived) ^{1}LC state may be bypassed, while the stronger spin-orbit coupling in the copper complex compared to the bare olefin promotes efficient ISC. Additionally, the copper center likely serves as a template by holding the two monomers in position prior to excitation, though this latter function must be verified by careful quantum yield measurements. Once the ^{3}LC state is occupied, the cycloaddition reaction occurs on the time scale of a few μs.

Surprisingly, the dimerization of cyclohexene under the same conditions proceeds through an entirely distinct reaction mechanism that does not involve any charge transfer between the copper and the ligand(s). Although the XTA and OTA results presented here cannot unambiguously identify the intermediates in this reaction, all our observations are consistent with the mechanism proposed by Salomon and Kochi, in which absorption of a photon drives the *cis-trans* isomerization of a cyclohexene ligand to provide the reactive species. These results demonstrate that it is possible to take advantage of at least two starkly divergent photocycloaddition pathways using a Cu(I) catalyst and potentially even choose which pathway a particular reaction follows through judicious choice of substrate(s). We expect that these insights will inspire efforts to broaden the scope of both inter- and intramolecular photocycloaddition reactions while also steering them toward the desired stereo- and/or regioisomer(s) of interest.

ASSOCIATED CONTENT

Supporting Information. General, XTA, and OTA experimental methods, decay-associated analysis methods, ^{1}H NMR spectra and kinetic fits, steady-state optical and X-ray spectra, and estimate of XTA excited state fractions. This material is available free of charge via the Internet at http://pubs.acs.org.

AUTHOR INFORMATION

Corresponding Author

* Dugan Hayes, Department of Chemistry, University of Rhode Island, Kingston, Rhode Island 02881, United States. Email: dugan@uri.edu

Notes

The authors declare no competing financial interest.

ACKNOWLEDGMENT

This material is based upon work supported by the National Science Foundation under Grant No. 1832944, which supported all XTA work by G.K.J, C.A., M.A.S., and D.H. Acknowledgment is made to the Donors of the American Chemical Society Petroleum Research Fund for support of this research, which supported all OTA work by G.K.J., C.A., and D.H. This material is based upon work supported by the U.S. Department of Energy, Office of Science, Office of Basic Energy Sciences, under Award DE-SC0019429, which supported all XTA work by J.E., N.G., and B.T.Y. This research used resources of the Advanced Photon Source, a U.S. Department of Energy (DOE) Office of Science User Facility operated for the DOE Office of Science by Argonne National Laboratory under Contract No. DE-AC02-06CH11357. All XTA data was collected at beamline 11-ID-D at the Advanced Photon Source, Argonne National Laboratory.

ABBREVIATIONS

XTA, X-ray transient absorption; OTA, optical transient absorption; XANES, X-ray absorption near-edge structure; MLCT, metal-to-ligand charge transfer; LMCT, ligand-to-metal charge transfer; LC, ligand-centered; OTf, trifluoromethanesulfonate; nb, norbornene; ch, cyclohexene; ISC, intersystem crossing; GSB, ground state bleach; ESA, excited state absorption.

REFERENCES

(1) Poplata, S.; Tröster, A.; Zou, Y. Q.; Bach, T. Recent Advances in the Synthesis of Cyclobutanes by Olefin [2 +2] Photocycloaddition Reactions. *Chemical Reviews* **2016**, *116* (17), 9748–9815. https://doi.org/10.1021/acs.chemrev.5b00723.

(2) Iriondo-Alberdi, J.; Greaney, M. F. Photocycloaddition in Natural Product Synthesis. *European Journal of Organic Chemistry* **2007**, *2007* (29), 4801–4815. https://doi.org/10.1002/ejoc.200700239.

(3) Bach, T.; Hehn, J. P. Photochemical Reactions as Key Steps in Natural Product Synthesis. *Angewandte Chemie International Edition* **2011**, *50* (5), 1000–1045. https://doi.org/10.1002/anie.201002845.

(4) Sarkar, D.; Bera, N.; Ghosh, S. [2+2] Photochemical Cycloaddition in Organic Synthesis. *European Journal of Organic Chemistry* **2020**, *2020* (10), 1310–1326. https://doi.org/10.1002/ejoc.201901143.

(5) Corey, E. J.; Mitra, R. B.; Uda, H. Total Synthesis of d,l-Caryophyllene and d,l-Isocaryophyllene. *Journal of the American Chemical Society* **1964**, *86* (3), 485–492. https://doi.org/10.1021/ja01057a040.

(6) Eaton, P. E.; Cole, T. W. Cubane. *J. Am. Chem. Soc.* **1964**, *86* (15), 3157–3158. https://doi.org/10.1021/ja01069a041.

(7) Jiang, Y.; Wang, C.; Rogers, C. R.; Kodaimati, M. S.; Weiss, E. A. Regio- and Diastereoselective Intermolecular [2+2] Cycloadditions Photocatalysed by Quantum Dots. *Nature Chemistry* **2019**, *11* (11), 1034–1040. https://doi.org/10.1038/s41557-019-0344-4.

(8) Skubi, K. L.; Swords, W. B.; Hofstetter, H.; Yoon, T. P. LED-NMR Monitoring of an Enantioselective Catalytic [2+2] Photocycloaddition. *ChemPhotoChem* **2020**, *4* (9), 685–690. https://doi.org/10.1002/cptc.202000094.

(9) Salomon, R. G.; Kochi, J. K. Copper(I) Catalysis in Photocycloadditions. I. Norbornene. *Journal of the American Chemical Society* **1974**, *96* (4), 1137–1144. https://doi.org/10.1021/ja00811a030.

(10) Flores, D. M.; Schmidt, V. A. Intermolecular 2 + 2 Carbonyl-Olefin Photocycloadditions Enabled by Cu(I)-Norbornene MLCT. *Journal of the American Chemical Society* **2019**, *141* (22), 8741–8745. https://doi.org/10.1021/jacs.9b03775.

(11) Salomon, R. G.; Folting, K.; Streib, W. E.; Kochi, J. K. Copper(I) Catalysis in Photocycloadditions. II. Cyclopentene, Cyclohexene, and Cycloheptene. *J. Am. Chem. Soc.* **1974**, *96* (4), 1145–1152. https://doi.org/10.1021/ja00811a031.

(12) Ghosh, S.; Raychaudhuri, S. R.; Salomon, R. G. Copper(I) Catalysis of Olefin Photoreactions. 15. Synthesis of Cyclobutanated Butyrolactones via Copper(I)-Catalyzed Intermolecular Photocycloadditions of Homoallyl Vinyl or Diallyl Ethers. *J. Org. Chem.* **1987**, *52* (1), 83–90. https://doi.org/10.1021/jo00377a015.

(13) Trecker, D. J.; Henry, J. P.; McKeon, J. E. Photodimerization of Metal-Complexed Olefins. *J. Am. Chem. Soc.* **1965**, *87* (14), 3261–3263. https://doi.org/10.1021/ja01092a056.

(14) Trecker, D. J.; Foote, R. S.; Henry, J. P.; McKeon, J. E. Photochemical Reactions of Metal-Complexed Olefins. II.

Dimerization of Norbornene and Derivatives. *J. Am. Chem. Soc.* **1966**, *88*, 3021–3026.
(15) Salomon, R. G.; Kochi, J. K. Copper(I) Triflate: A Superior Catalyst for Olefin Photodimerization. *Tetrahedron Lett.* **1973**, *14*, 2529–2532.
(16) Whitesides, G. M.; Goe, G. L.; Cope, A. C. Irradiation of Cis,Cis-1,5-Cyclooctadiene in the Presence of Copper(I) Chloride. *J. Am. Chem. Soc.* **1969**, *91* (10), 2608–2616. https://doi.org/10.1021/ja01038a036.
(17) Salomon, R. G. Homogeneous Metal-Catalysis in Organic Photochemistry. *Tetrahedron* **1983**, *39* (4), 485–575. https://doi.org/10.1016/S0040-4020(01)91830-7.
(18) Salomon, R. G.; Sinha, A.; Salomon, M. F. Copper(I) Catalysis of Olefin Photoreactions. Photorearrangement and Photofragmentation of Methylenecyclopropanes. *J. Am. Chem. Soc.* **1978**, *100* (2), 520–526. https://doi.org/10.1021/ja00470a027.
(19) Geiger, D.; Ferraudi, G. Photochemistry of Cu-Olefin Complexes: A Flash Photochemical Investigation of the Reactivity of Cu(Ethylene)+ and Cu(Cis,Cis-1,5-Cyclooctadiene)+2. *Inorganica Chimica Acta* **1985**, *101* (3), 197–201. https://doi.org/10.1016/S0020-1693(00)87654-9.
(20) Budzellar, P. H. M.; Timmermans, P. J. J. A.; Mackor, A.; Baerends, E. J. Bonding in the Ground State and Excited States of Copper-Alkene Complexes. *Journal of Organometallic Chemistry* **1987**, *331* (3), 397–407. https://doi.org/10.1016/0022-328X(87)80011-6.
(21) Schuster, D. I.; Dunn, D. A.; Heibel, G. E.; Brown, P. B.; Rao, J. M.; Woning, J.; Bonneau, R. Enone Photochemistry. Dynamic Properties of Triplet Excited States of Cyclic Conjugated Enones as Revealed by Transient Absorption Spectroscopy. *J. Am. Chem. Soc.* **1991**, *113* (16), 6245–6255. https://doi.org/10.1021/ja00016a048.
(22) Cucarull-González, J. R.; Hernando, J.; Alibés, R.; Figueredo, M.; Font, J.; Rodríguez-Santiago, L.; Sodupe, M. [2 + 2] Photocycloaddition of 2(5H)-Furanone to Unsaturated Compounds. Insights from First Principles Calculations and Transient-Absorption Measurements. *J. Org. Chem.* **2010**, *75* (13), 4392–4401. https://doi.org/10.1021/jo100341a.
(23) Maturi, M. M.; Wenninger, M.; Alonso, R.; Bauer, A.; Pöthig, A.; Riedle, E.; Bach, T. Intramolecular [2+2] Photocycloaddition of 3- and 4-(But-3-Enyl)Oxyquinolones: Influence of the Alkene Substitution Pattern, Photophysical Studies, and Enantioselective Catalysis by a Chiral Sensitizer. *Chemistry – A European Journal* **2013**, *19* (23), 7461–7472. https://doi.org/10.1002/chem.201300203.
(24) Logan, S. R. Does a Photochemical Reaction Have a Reaction Order? *J. Chem. Educ.* **1997**, *74* (11), 1303. https://doi.org/10.1021/ed074p1303.
(25) Salomon, R. G.; Kochi, J. K. Cationic Olefin Complexes of Copper(I). Structure and Bonding in Group Ib Metal-Olefin Complexes. *J. Am. Chem. Soc.* **1973**, *95* (6), 1889–1897. https://doi.org/10.1021/ja00787a031.
(26) Chen, L. X.; Zhang, X. Photochemical Processes Revealed by X-Ray Transient Absorption Spectroscopy. *J. Phys. Chem. Lett.* **2013**, *4* (22), 4000–4013. https://doi.org/10.1021/jz401750g.
(27) Kau, L. S.; Spira-Solomon, D. J.; Penner-Hahn, J. E.; Hodgson, K. O.; Solomon, E. I. X-Ray Absorption Edge Determination of the Oxidation State and Coordination Number of Copper. Application to the Type 3 Site in Rhus Vernicifera Laccase and Its Reaction with Oxygen. *J. Am. Chem. Soc.* **1987**, *109* (21), 6433–6442. https://doi.org/10.1021/ja00255a032.
(28) Rudolph, J.; Jacob, C. R. Revisiting the Dependence of Cu K-Edge X-Ray Absorption Spectra on Oxidation State and Coordination Environment. *Inorg. Chem.* **2018**, *57* (17), 10591–10607. https://doi.org/10.1021/acs.inorgchem.8b01219.
(29) Benfatto, M.; Natoli, C. R.; Bianconi, A.; Garcia, J.; Marcelli, A.; Fanfoni, M.; Davoli, I. Multiple-Scattering Regime and Higher-Order Correlations in x-Ray-Absorption Spectra of Liquid Solutions. *Phys. Rev. B* **1986**, *34* (8), 5774–5781. https://doi.org/10.1103/PhysRevB.34.5774.
(30) Bianconi, A.; Li, C.; Campanella, F.; Longa, S. D.; Pettiti, I.; Pompa, M.; Turtù, S.; Udron, D. Cu K-Edge Polarized x-Ray-Absorption near-Edge Structure of Bi2CaSr2Cu2O8. *Phys. Rev. B* **1991**, *44* (9), 4560–4569. https://doi.org/10.1103/PhysRevB.44.4560.
(31) Choy, J.-H.; Yoon, J.-B.; Jung, H. Polarization-Dependent X-Ray Absorption Spectroscopic Study of [Cu(Cyclam)]2+-Intercalated Saponite. *J. Phys. Chem. B* **2002**, *106* (43), 11120–11126. https://doi.org/10.1021/jp020374+.
(32) Sano, M.; Komorita, S.; Yamatera, H. XANES Spectra of Copper(II) Complexes: Correlation of the Intensity of the 1s → 3d Transition and the Shape of the Complex. *Inorg. Chem.* **1992**, *31* (3), 459–463. https://doi.org/10.1021/ic00029a022.
(33) Mara, M. W.; Fransted, K. A.; Chen, L. X. Interplays of Excited State Structures and Dynamics in Copper(I) Diimine Complexes: Implications and Perspectives. *Coordination Chemistry Reviews* **2015**, *282*, 2–18. https://doi.org/10.1016/j.ccr.2014.06.013.
(34) Penfold, T. J.; Karlsson, S.; Capano, G.; Lima, F. A.; Rittmann, J.; Reinhard, M.; Rittmann-Frank, M. H.; Braem, O.; Baranoff, E.; Abela, R.; Tavernelli, I.; Rothlisberger, U.; Milne, C. J.; Chergui, M. Solvent-Induced Luminescence Quenching: Static and Time-Resolved X-Ray Absorption Spectroscopy of a Copper(I) Phenanthroline Complex. *J. Phys. Chem. A* **2013**, *117* (22), 4591–4601. https://doi.org/10.1021/jp403751m.
(35) Tomson, N. C.; Williams, K. D.; Dai, X.; Sproules, S.; DeBeer, S.; Warren, T. H.; Wieghardt, K. Re-Evaluating the Cu K Pre-Edge XAS Transition in Complexes with Covalent Metal–Ligand Interactions. *Chem. Sci.* **2015**, *6* (4), 2474–2487. https://doi.org/10.1039/C4SC03294B.
(36) Walroth, R. C.; Uebler, J. W. H.; Lancaster, K. M. Probing CuI in Homogeneous Catalysis Using High-Energy-Resolution Fluorescence-Detected X-Ray Absorption Spectroscopy. *Chem. Commun.* **2015**, *51* (48), 9864–9867. https://doi.org/10.1039/C5CC01827G.
(37) Bair, R. A.; Goddard, W. A. Ab Initio Studies of the X-Ray Absorption Edge in Copper Complexes. I. Atomic Cu2+ and Cu(II)Cl2. *Phys. Rev. B* **1980**, *22* (6), 2767–2776. https://doi.org/10.1103/PhysRevB.22.2767.
(38) Yokoyama, T.; Kosugi, N.; Kuroda, H. Polarized Xanes Spectra of CuCl2 · 2H2O. Further Evidence for Shake-down Phenomena. *Chemical Physics* **1986**, *103* (1), 101–109. https://doi.org/10.1016/0301-0104(86)85106-0.
(39) Jou, F. Y.; Dorfman, L. M. Pulse Radiolysis Studies. XXI. Optical Absorption Spectrum of the Solvated Electron in Ethers and in Binary Solutions of These Ethers. *The Journal of Chemical Physics* **2003**, *58* (11), 4715. https://doi.org/10.1063/1.1679050.
(40) Tran-Thi, T. H.; Koulkes-Pujo, A. M. Electron and Organic Radical Anion Solvation. Pulse Radiolysis of Tetrahydrofuran and Its Solutions of N-Methylacetamide or Pyrrolidone. *J. Phys. Chem.* **1983**, *87* (7), 1166–1169. https://doi.org/10.1021/j100230a014.
(41) Martini, I. B.; Barthel, E. R.; Schwartz, B. J. Mechanisms of the Ultrafast Production and Recombination of Solvated Electrons in Weakly Polar Fluids: Comparison of Multiphoton Ionization and Detachment via the Charge-Transfer-to-Solvent Transition of Na− in THF. *The Journal of Chemical Physics* **2000**, *113* (24), 11245. https://doi.org/10.1063/1.1328071.
(42) Iwamura, M.; Takeuchi, S.; Tahara, T. Real-Time Observation of the Photoinduced Structural Change of Bis(2,9-Dimethyl-1,10-Phenanthroline)Copper(I) by Femtosecond Fluorescence Spectroscopy: A Realistic Potential Curve of the Jahn–Teller Distortion. *J. Am. Chem. Soc.* **2007**, *129* (16), 5248–5256. https://doi.org/10.1021/ja069300s.
(43) Shaw, G. B.; Grant, C. D.; Shirota, H.; Castner, E. W.; Meyer, G. J.; Chen, L. X. Ultrafast Structural Rearrangements in the MLCT Excited State for Copper(I) Bis-Phenanthrolines in Solution. *J. Am. Chem. Soc.* **2007**, *129* (7), 2147–2160. https://doi.org/10.1021/ja067271f.
(44) Iwamura, M.; Takeuchi, S.; Tahara, T. Ultrafast Excited-State Dynamics of Copper(I) Complexes. *Acc. Chem. Res.* **2015**, *48* (3), 782–791. https://doi.org/10.1021/ar500353h.

(45) Paul J. Kropp, John J. Snyder, Peter C. Rawlings, and Harold G. Fravel, Jr. Photochemistry of Cycloalkenes. Photodimerization of Cyclohexene. *Journal of Organic Chemistry* **1980**, *45*, 4471–4474.
(46) Ganis, P.; Lepore, U.; Martuscelli, E. Crystal and Molecular Structure of Di-μ-Chlorotris(Trans-Cyclooctene)Dicopper(I). *J. Phys. Chem.* **1970**, *74* (12), 2439–2444. https://doi.org/10.1021/j100706a004.
(47) Evers, J. T. M.; Mackor, A. Photocatalysis IV. Preparation and Characterization of a Stable Copper(I) Triflate·trans-Cycloheptene Complex. *Recueil des Travaux Chimiques des Pays-Bas* **1979**, *98* (6), 423–423. https://doi.org/10.1002/recl.19790980614.
(48) Cope, A. C.; Ganellin, C. R.; Johnson, H. W.; Van Auken, T. V.; Winkler, H. J. S. Molecular Asymmetry of Olefins. I. Resolution of Trans-Cyclooctene. *J. Am. Chem. Soc.* **1963**, *85* (20), 3276–3279. https://doi.org/10.1021/ja00903a049.
(49) Royzen, M.; Yap, G. P. A.; Fox, J. M. A Photochemical Synthesis of Functionalized Trans-Cyclooctenes Driven by Metal Complexation. *J. Am. Chem. Soc.* **2008**, *130* (12), 3760–3761. https://doi.org/10.1021/ja8001919.
(50) Verbeek, J.; Van Lenthe, J. H.; Timmermans, P. J. J. A.; Mackor, A.; Budzelaar, P. H. M. On the Existence of Trans-Cyclohexene. *J. Org. Chem.* **1987**, *52* (13), 2955–2957. https://doi.org/10.1021/jo00389a067.
(51) Rencken, I.; Orchard, S. W. Formation Constants of Copper(I) Chloride Complexes with Cis,Cis-1,5-Cyclooctadiene and Other Cyclic Olefins. *Inorg. Chem.* **1986**, *25* (12), 1972–1976. https://doi.org/10.1021/ic00232a014.
(52) Hartley, F. R. Thermodynamic Data for Olefin and Acetylene Complexes of Transition Metals. *Chem. Rev.* **1973**, *73* (2), 163–189. https://doi.org/10.1021/cr60282a005.
(53) Felker, P. M.; Zewail, A. H. Rates of Photoisomerization of Trans-Stilbene in Isolated and Solvated Molecules: Experiments on the Deuterium Isotope Effect and RRKM Behavior. *J. Phys. Chem.* **1985**, *89* (25), 5402–5411. https://doi.org/10.1021/j100271a018.
(54) Bloh, J. Z. A Holistic Approach to Model the Kinetics of Photocatalytic Reactions. *Frontiers in Chemistry* **2019**, *7*, 128. https://doi.org/10.3389/fchem.2019.00128.

For Table of Contents Only